

# A Computation-Efficient CNN System for High-Quality Brain Tumor Segmentation

Yanming Sun, Chunyan Wang

**Abstract**—In this paper, a Convolutional Neural Network (CNN) system is proposed for brain tumor segmentation. The system consists of three parts, a pre-processing block to reduce the data volume, an application-specific CNN(ASCNN) to segment tumor areas precisely, and a refinement block to detect/remove false positive pixels. The CNN, designed specifically for the task, has 7 convolution layers, 16 channels per layer, requiring only 11716 parameters. The convolutions combined with max-pooling in the first half of the CNN are performed to localize tumor areas. Two convolution modes, namely depthwise convolution and standard convolution, are performed in parallel in the first 2 layers to extract elementary features efficiently. For a fine classification of pixel-wise precision in the second half of the CNN, the feature maps are modulated by adding the weighted local features generated in the first half of the CNN. The performance of the proposed system has been evaluated by an online platform with dataset BRATS2018. Requiring a very low computation volume, the proposed system delivers a high segmentation quality indicated by its average Dice scores of 0.75, 0.88 and 0.76 for enhancing tumor, whole tumor and tumor core, respectively, and the median Dice scores of 0.85, 0.92, and 0.86. The consistency in system performance has also been measured, demonstrating that the system is able to reproduce almost the same output to the same input after retraining. The simple structure of the proposed system facilitates its implementation in computation restricted environment, and a wide range of applications can thus be expected.

**Index Terms**—Application-specific convolutional neural network (ASCNN), brain tumor segmentation, machine learning, 2D filtering.

## I. INTRODUCTION

**B**RAIN tumors pose a serious problem to human health, and brain tumor segmentation is a critical step for the diagnosis and treatment of the disease. Manual segmentation is very time-consuming and often causes delays. It is thus important to develop fully automated systems for brain tumor segmentation to facilitate timely diagnosis.

The automated brain tumor segmentation is a very challenging task. First of all, a human brain is very complex 3D structure. From computer vision point of view, it is not easy to distinguish tumor tissues from healthy tissues, whereas the shapes, sizes, textures and locations of brain tumors are very different from patient to patient. Moreover, a high quality of brain tumor segmentation is required for its meaningful

applications in diagnosis. This quality requirement is not only in the voxel-wise precision to define whole tumor regions, but also in a fine classification of the voxels into three types of intra-tumoral structures, namely edema, non-enhancing (solid) core/necrotic (or fluid-filled) core and enhancing core [1].

Brain tumor segmentation can be done by means of filtering and/or morphological operations. The segmentation method reported in [2] is based on feature extracted by means of Sobel high-pass filtering. Tumor features can also be extracted by applying Gabor filters, and the data are used to classify the pixels with extremely randomized trees [3]. As healthy brains have certain degree of symmetry [4], brain tumor detection can also be done by analysing the symmetry of brain images [5]. Implementations of these methods do not require large number of computation resources. However, owing to the complexity of the brain tumor variations, it is difficult to precisely classify the pixels of intra-tumoral structures by simple filtering methods.

Convolutional Neural Network (CNN) can extract various features from input images if it is trained with sufficiently comprehensive samples, and thus it has potential to deal with the variations of tumors in brain images with a view to handling the challenge of automated brain tumor segmentation.

U-net, designed based on FCN [6], has been widely used in medical image processing, including brain tumor segmentation [7]. U-net performs filtering operations combined first with downsampling operations and then with upsampling operations, and the feature maps generated in the early layers are concatenated with those of the late layers. A number of U-net-based CNN systems for brain tumor segmentation have been reported in recent years, attempting to improve the segmentation quality. In the CNN presented in [8], standard convolution blocks in the original U-net are replaced by inception blocks. U-net structure can also be used as a basic unit, and multiple units are stacked to seek a better processing quality [9]. In DRINet [10], standard convolution blocks in the first layers are replaced by dense connection blocks, and those in the last layers are replaced by residual inception blocks, in which the operations are performed without concatenating feature maps produced by the early layers. The network presented in [11] was designed to have recombination of features and spatially adaptive recalibration block to improve the segmentation quality.

This work was supported in part by Compute Canada and in part by the Natural Sciences and Engineering Research Council (NSERC) of Canada. Yanming Sun is with the Department of Electrical and Computer Engineering, Concordia University, Montreal, QC, H3G 1M8, Canada (e-mail: S\_YANMIN@encs.concordia.ca)

Chunyan Wang is with the Department of Electrical and Computer Engineering, Concordia University, Montreal, QC, H3G 1M8, Canada (e-mail: chunyan@ece.concordia.ca)

Other forms of CNN have also been adopted for brain tumor segmentation. In the network reported in [12], the structure of deep residual network is used and combines with spatial fusion blocks. The network in [13] is an architecture of multiple convolution pathways, and it is made to operate with patches obtained from axial, coronal, and sagittal views of the 3D MRI brain images. DeepMedic [14] and DF-MLDeepMedic network [15] are CNNs with two convolution pathways, to extract local and larger contextual features, respectively. It should be noted that, the convolutions in these two systems are performed with 3D input data, and thus 4D kernels are used in a convolution involving multiple channels, which requires more parameters to be trained with respect to standard 2D convolution.

In general, the CNN systems require much more computation resources than those of deterministic filtering systems. An improvement of processing quality is often obtained at the expense of more computation cost. It should, however, be noted that a requirement of intensive computation can limit the implementation the systems, which, in turn, may make them less applicable.

The objective of the work presented in this paper is to design a high-quality CNN system for brain tumor segmentation with low-computation requirement in order to facilitate its implementation. The system is composed of three parts, pre-processing block, CNN, and refinement block. The pre-processing is to reduce the input data volume to facilitate the computation of the system. The CNN is designed specifically according to the characters of the data in brain images, aiming at efficient feature extraction and precise classification. The refinement is to remove possible false positive voxels.

The paper consists of 4 sections. The detailed description of the system design is found in Section II, and those of the training and testing is presented in Section III. A performance comparison is also found in Section III.

## II. PROPOSED SYSTEM

Automated brain tumor segmentation is an important processing for timely diagnosis in order to optimize treatments. In the design of the proposed system, the emphasis is to achieve

a good segmentation quality at the lowest computation cost in order to facilitate its implementation. The basic block diagram of the system is shown in Fig. 1.

The input of the proposed system is 3D brain images. The case of each patient is represented by four 3D images, namely FLAIR, T1, T1c and T2, as shown in Fig. 1. Each of the 3D images is sliced into 2D slices. Hence, a voxel in a 3D image becomes a pixel in a 2D slice, and the brain tumor segmentation of 3D images is done by segmenting these 2D slices. An example of the 2D slices is shown in Fig. 2. (a)~(d), and the ground truth of the brain tumor segmentation corresponding to these slices is shown in Fig. 2 (e). It is difficult to find a deterministic model that can be used to detect various brain tumors in a pixel-wise precision. CNN can be potentially useful to handle such a problem if there is an appropriate dataset for training and testing the system.

In general, CNN systems require a very large amount of computation. In this design, a simple CNN is proposed to detect various features of brain tumors and segment different forms of brain tumor areas. To facilitate the computation in the CNN, pre- and post-processing blocks are used, as shown in Fig. 1. The functions of the three parts are as follow.

1. Pre-processing. It is to reduce the volume of input data applied to the succeeding CNN, without any risk of losing feature data of brain tumors.
2. CNN. It is composed of filtering layers to detect features of brain tumors and generate maps indicating the pixels of candidates of brain tumors in each 2D slice.
3. Post-processing. It is to remove possible false positive pixels.

The detail of the design of these parts are presented in the following sub-sections.

### A. Pre-processing – Data Reduction

The system is designed to operate with 3D brain images. The pre-processing block is made to reduce the data volume of the 3D images to facilitate the computations in the CNN. The dimensions of the 3D images from commonly used datasets, such as BRATS2017 and BRATS2018, are  $240 \times 240 \times 155$ , resulting from a post-acquisition registration.

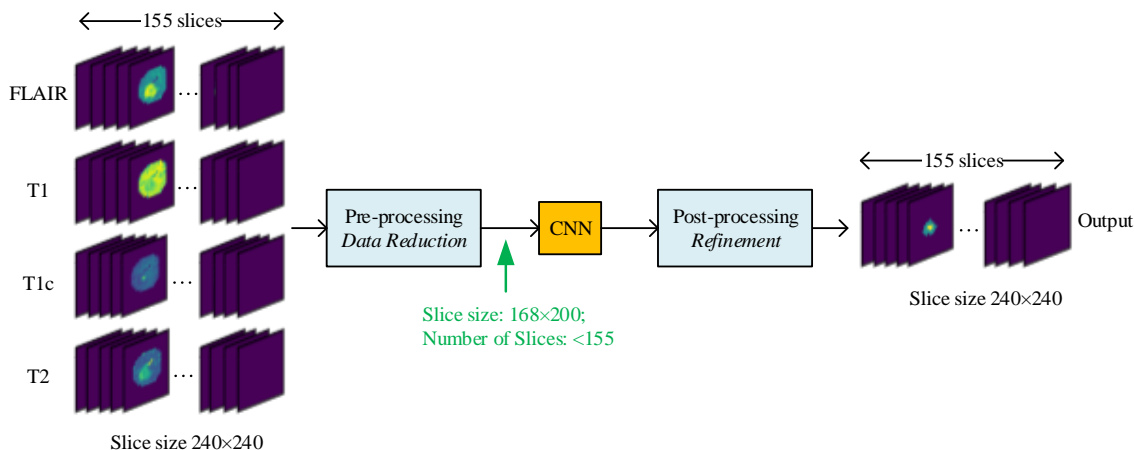


Fig. 1. Overview of the proposed 3-block system. There are four 3D images namely FLAIR, T1, T1c and T2 in each patient case and the size of each 3D image is  $240 \times 240 \times 155$ .

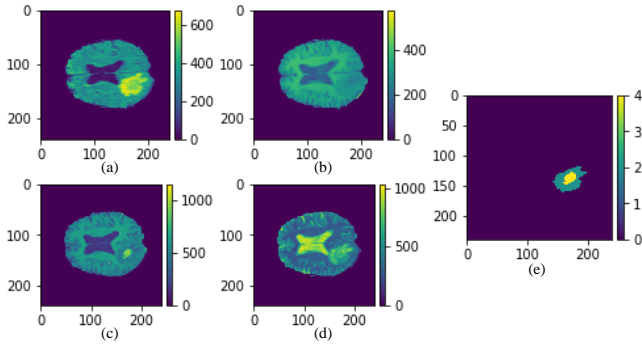


Fig. 2. (a) FLAIR slice. (b) T1 slice. (c) T1c slice. (d) T2 slice. (e) Ground truth.

The brain image segmentation is, in fact, to identify the pixels in different tumor areas. As a result, the tumor-free brain areas will merge with the background and the pixels in these locations will be classified in the same tumor-free class. Evidently, a large majority of the pixels are found in this class, and some of them can be very easily identified. Excluding these pixels, or a large part of them, from the operations in the CNN will significantly reduce the amount of data to be processed without causing any signal loss, which will result in not only a better computation efficiency but also a lower risk of false positive result.

In the pre-processing block, the reduction of the data volume is done effectively with a very insignificant amount of computation, thanks to the 2 facts. Firstly, there is a wide margin in each side of a brain slice. Excessive margins can be easily identified and removed. Secondly, out of the 155 slices in each 3D image, some slices are free of tumor areas and they can be removed without affecting the quality of the segmentation.

The pre-processing is done in 2 steps. The first step is to remove the excessive margins in each slice, and the second is to identify and remove tumor-free slices. The details in the design are found in the following sub-sections.

### 1) Detection and Removal of Excessive Margins in Slices

In each slice of a 3D brain image, the brain area occupies only a small portion of the space, due to a wide margin in each side, and such an example is shown in Fig. 3 (a). It is very easy to detect the widths of the 4 margins, as the pixels in the background have the gray-level of zero. The preprocessing is to cut off excessive margins in order to reduce the size of the slices.

Let  $x_1$  denote the distance between the left boundary of a slice and the leftmost point of the brain area,  $x_2$ ,  $y_1$  and  $y_2$  denote the distances, respectively, to the other three boundaries of the slice, as shown in Fig. 3 (a). The values of  $x_1$ ,  $x_2$ ,  $y_1$  and  $y_2$  change from slice to slice. Let  $x_{1m}$ ,  $x_{2m}$ ,  $y_{1m}$  and  $y_{2m}$ , to be the widths of the 4 rectangle margins to be cut-off. Their values are determined by the minimum distances found in all the slices of the 3D images in order to apply them to all these slices without risk of data loss due to over-cutting.

In case of using the dataset BRATS2018,  $x_{1m}$ ,  $x_{2m}$ ,  $y_{1m}$  and  $y_{2m}$  are chosen to be 26, 14, 36 and 36, respectively, and the size of

the slices is reduced from  $240 \times 240$  to  $168 \times 200$  after the removal, as the example showed in Fig. 3 (b). The reduction of the data volume in this case is 42%. This simple procedure can be applied to the input from different datasets to reduce significantly the computation volume in CNN processes.

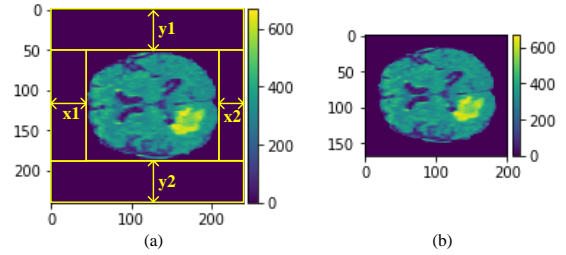


Fig. 3. (a) Example of the original input slices sized  $240 \times 240$  pixels. (b) Slice after the removal of excessive margins, sized  $168 \times 200$  pixels.

### 2) Detection and Removal of Tumor-Free Slices

There are three kinds of tumor-free slices in brain images.

1. In the sequence of the 155 slices in each 3D image, brain tumor areas are seldom found in the slices located at the 2 ends of the sequence. The slices of this kind can be identified by their very high percentage of background pixels. Two examples of such slices are shown in Fig. 4.
2. The slices of the second kind are of healthy section of a brain. Healthy brains have natural left-right symmetry, which is reflected to the upper-lower symmetry in brain images [16][17], as an example shown in Fig. 5 (a)(c). A tumor causes an asymmetry, as a slice with tumor shown in Fig. 5 (b)(d). The development of a brain tumor increases the asymmetry between the upper and lower halves of the slices. Thus, a tumor-free slice of the second kind can be identified by a high degree of upper-lower symmetry of the pixel data in the brain area.
3. Some slices have only incomplete brain areas appearing, as examples shown in Fig. 6 (a) and (b), due to imperfection in medical image acquisition. As these slices are located in the areas where it is very rare to find brain tumors, they are considered tumor-free. A slice of this kind may not have particularly high percentage of background pixels, but a significant asymmetry between the upper half and the lower halves of the brain outlines, as shown in Fig. 6 (c) and (d). Hence one can identify it by calculating the degree of symmetry of the outlines.

Evidently, a tumor-free slice can be identified by a simple method to detect (1) a very high percentage of background pixels, (2) a high degree of symmetry of pixel data in the upper-lower halves of the brain area, or (3) a low degree of symmetry of the upper-lower brain outlines. Once identified, it is removed from the input slices, as all of its pixels are in the tumor-free class, without need for computation.

There are various approaches to detect the similarity between the upper and lower halves of brain area contents or brain area outlines. Structural similarity (SSIM) [18] is one of the commonly used approach for this purpose. It involves the mean, variance and covariance in the calculation.

Applying the method to the samples from BRATS2018, one can find that the number of tumor-free slices per case is between

13 and 43, out of 155, which is not negligible. Combining it with the removal of the excessive margins in each slice, a reduction of more than 50% data volume can be achieved.

In conclusion, by cutting off the excessive margins in the slices and detecting/removing the tumor-free slices, one can expect a significant reduction of the data to be processed in the CNN stage.

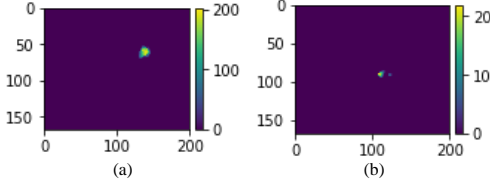


Fig. 4. Slices with high percentage of background pixels. They are the 8<sup>th</sup> and the 142<sup>nd</sup> slices from a 3D FLAIR image.

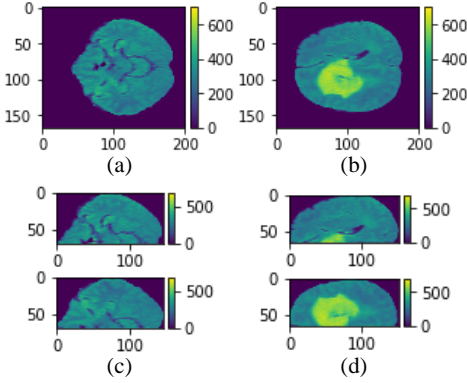


Fig. 5. (a) Slice without tumor, the 58<sup>th</sup> slice from a FLAIR image. (b) Slice with tumor, the 90<sup>th</sup> slice from a FLAIR image. (c) Upper and lower halves of the contents in (a). (d) Upper and lower halves of the contents in (b).

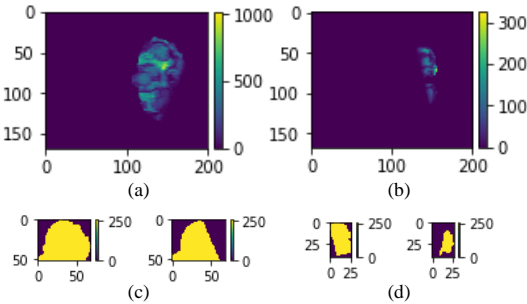


Fig. 6. (a) (b) examples of slices of incomplete brain areas. (c) Upper and lower halves of the binary image of (a) that highlights the outline of the brain area. (d) Upper and lower halves of the binary image of (b).

## B. CNN

The CNN has its input signal of four channels, given by the four 3D images, namely FLAIR, T1, T1c and T2, but the dimensions of the channels are smaller because of the pre-processing. Each of the four channels consists of 2D slices sized  $168 \times 200$  pixels and indexed from 1 to  $N_{st}$ . As the sizes of brains appearing in the 3D images are different,  $N_{st}$ , the number of slices per channel, can vary, e.g., from 119 to 149, depending on cases of patients. Fig. 7 (a)~(d) illustrates 4 slices of the same index number from the 4 input channels.

As mentioned previously, the function of the CNN is to identify the pixels in the four areas, namely the peritumoral edema (ED), the necrotic/non-enhancing tumor core (NCR/NET), the GD-enhancing tumor (ET), and the tumor-free

areas. The classification results are used to indicate the areas of whole tumor (WT), tumor core (TC) and enhancing tumor (ET) as shown in Fig. 7 (e).

In order to achieve a good segmentation accuracy at the lowest computation cost, instead of a general-purpose CNN, one needs an application-specific CNN (ASCNN), i.e., a CNN custom-designed for the task. To this end, an investigation of the input data is needed.

As the 3D brain images may not be acquired under the exactly same condition, the intensity range of the input data are not uniformed [19][20]. Thus, the input data needs to be normalized before being applied to the convolution layers. However, unlike batch normalizations commonly used in CNNs, this normalization needs to be “channel-wise”, performed to the data of each input channel, i.e.,  $N_{st}$  slices from each of the four 3D images of one given patient case. To be more specific, the data of each channel are normalized with the mean and the standard deviation of the channel. This kind of normalization unifies the data range of all the channels, while minimizing the risk of attenuating critical feature information in channels of low-intensity levels.

As mentioned previously, there are a lot of variations in brain images. From microscopic point of view, it is hard to differentiate the gray level variations in the tumor areas from those in healthy areas. However, from a macroscopic point of view, the tumor textures look somehow different from those in the healthy parts. Hence, the detection of that difference needs image features extracted from a relatively large neighborhood. Moreover, as a tumor can grow in any part of a brain, a division of a slice from a 3D brain image can result in a division of brain tumor neighborhoods, which may affect the quality of the texture detection. Therefore, the proposed CNN is designed to operate with undivided slices of 3D brain images.

Based on the investigation of the input data, the strategy of this design is for the CNN to perform 2 functions in sequence. First function is to extract elementary features and to localize brain tumor areas, and the second is a fine classification of the pixels in the areas. The former requires a detection of both “fine” signal variations and “coarse” brain tissue textures, and the latter needs local feature information in the tumor areas. To do so, a simple CNN is proposed as illustrated in Fig. 8. It is based on the main frame of U-net, but has some important differences in the design to achieve better performance without need for more computation.

The feature extraction is performed in the first three convolution layers and the operation in the 4th layer is to detect the tumor areas. The following considerations have been taken in the design of these layers.

1. It should be mentioned that the input image data of the four 3D images, namely FLAIR, T1, T1c and T2, are acquired with different emphases on different lesion areas of a specific brain. Though there is a correlation among the four 3D images, each of them contains enhanced features of particular intra-tumoral structures. To make good use of the signals from the four slices taken from the same brain section, two different modes of convolutions are used in the first 2 layers to extract various elementary features. As



shown in Fig. 8, in the upper part of the first 2 layers, so-called depthwise convolutions, represented by red-white-polka-dot rectangles, are applied to individual 2D slices. For example, in the first layer, there are four  $3\times 3$  kernels in the depthwise convolution and each of them is applied to the data of a single 2D slice to generate a 2D feature map representing the particular features of the slice. Each depthwise convolution is followed by a feature map normalization applied to each individual feature map. Standard convolutions, indicated by solid-red rectangles in the diagram, are also used to generate 2D feature maps, and each of these maps is based on the data originated from the 2D slices taken from the FLAIR, T1, T1c and T2 channels. The two kinds of convolutions are performed in parallel in the first 2 layers, as shown in Fig. 8, and the results are then concatenated before being applied to the 3rd convolution layer.

- Following each of the first 3 convolution layers, a pooling operation is performed to each of the 2D data maps, as shown in Fig. 8. It is to “zoom out” the 2D map, so that the effective size of neighbourhood in the succeeding convolution will be larger than the size of the convolution kernels of  $3\times 3$  pixels. After the 3 layers of  $3\times 3$  convolution followed by pooling, the operation in the 4th layer will be performed with the input data originated from a quite large neighbourhood, i.e., in a quasi “macroscopic” scale.
- As each pooling operation is performed to the convolved data that are more likely the results of high-pass filtering, max pooling is the most suitable to minimize the information loss while the data volume being reduced significantly. It is also used to increase the information density of the data applied to the succeeding convolution layers.

The function of the first 4 layers combined can be seen as a coarse classification of tumor pixels and tumor-free ones. As the signal resolution is reduced by the pooling operations whereas the segmentation requires a pixel-wise precision, the second part of the proposed CNN is designed to have the following 2 characters.

- Upsampling operations are performed so that the dimensions of the output maps will grow to be the same as those of the input slices of the CNN. Bilinear upsampling is used for this purpose. However, the upsampling does not improve the precision of image signal.
- To precisely classify the pixels in each slice, the filtering results of the first convolution layers, i.e. local feature data, are included in the convolutions of the last 3 layers. Instead of concatenation, these data are first scaled by trainable coefficients and then added to the upsampled data, as shown in Fig. 8. This addition can be seen as a modulation of the upsampled data by the local feature data, or vice versa. It results in an enhancement of the feature data in tumor areas, which implies an attenuation of those in tumor-free areas. Hence the filtering operations in the last 3 convolution layers are performed to the data well prepared with pertinent feature information of brain tumors for a fine classification.

The proposed CNN is designed specifically to suit characters of the input signals to optimize the filtering operations with a view to achieving a good processing quality at the lowest computation cost. In fact, the specific measures taken to improve the processing quality are all helping to reduce the computation complexity: Half of the convolutions in the first 2 layers are “depthwise”, requires only  $1/n$  of computation, compared with standard convolutions, where  $n$  is the number of the input channels. In the second half of the CNN, the additions, instead of concatenations, of the filtered data from earlier layers and the upsampled data yields another very significant reduction of computation volume.

As the input data in each layer are well prepared for an efficient filtering operation, the proposed CNN has only 7 convolution layers and each generates sixteen 2D maps, except the last one, as shown in Fig. 8. The details of the CNN configuration are presented in Table I. The total number of parameters of the network is 11716. It is likely the simplest U-net-based CNN for brain tumor segmentation. With this low computation complexity, the network can be very easily trained and implemented in a recourse-restricted environment.

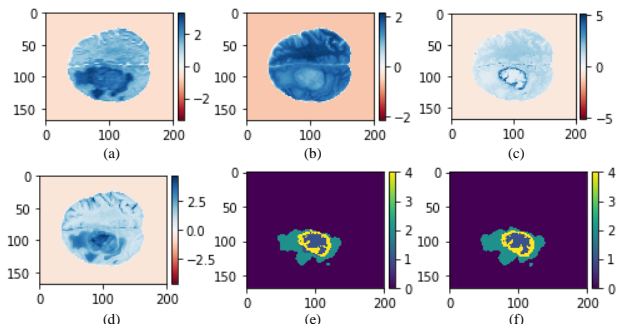


Fig. 7. Example of the input and output of the proposed CNN. (a)–(d) FLAIR, T1, T1c, and T2 slice samples. In each slice, the intensity values are channel-wisely normalized. (e) Ground truth. (f) Example of predicted result.

TABLE I  
DETAILS OF THE CNN CONFIGURATION

Layer	Kernel Size	Number of input channels	Number of output channels	Size of input channel	Size of output channel
1	$3\times 3$	4	16	$168\times 200$	$84\times 100$
2	$3\times 3$	16	16	$84\times 100$	$42\times 50$
3	$3\times 3$	16	16	$42\times 50$	$21\times 25$
4	$3\times 3$	16	16	$21\times 25$	$42\times 50$
5	$3\times 3$	16	16	$42\times 50$	$84\times 100$
6	$3\times 3$	16	16	$84\times 100$	$168\times 200$
7	$3\times 3$	16	4	$168\times 200$	$168\times 200$

### C. Post-Processing - Refinement

After the classification by the CNN, the post-processing block is placed to identify the pixels that are falsely classified as positive ones. The identification is based on the fact that a brain tumor and its enhanced tumor core, if it exists, are 3D objects, and the area of each of them must be found in a certain number of consecutive slices.

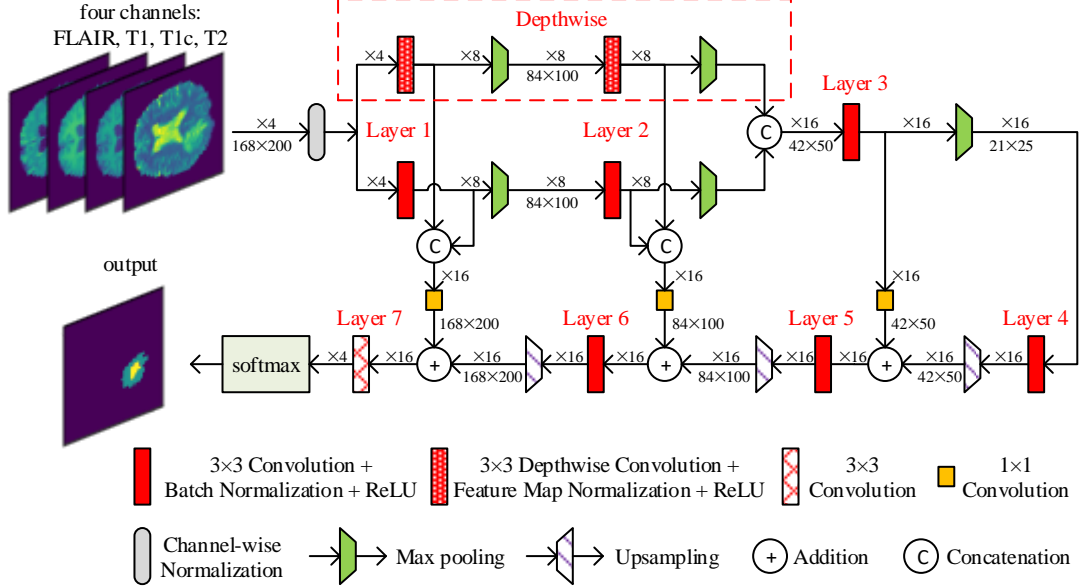


Fig. 8. Detailed diagram of the proposed CNN.

The thickness of a detectable whole tumor is considered to be at least  $1/20$  of the diameter of a brain. If a 3D brain image consists of 155 slices, this thickness corresponds to at least seven consecutive slices. If a whole tumor area appears in fewer than seven consecutive slices, the pixels in this area are likely falsely classified, and will be re-classified as tumor-free pixels.

The identification of the false-positive pixels of enhancing tumor core is based on a similar principle that tumor cores have their own minimum size limit. Also, it is common sense that the minimum size of a tumor core is slightly smaller than that of a whole tumor. If a predicted tumor core area appears in fewer than six consecutive slices, instead of seven, the pixels in the area will be considered false-positive and then be reclassified as non-enhancing tumor pixels.

By applying the principles mentioned above, the post-processing block improves the precision of segmentation without adding a perceivable amount of computation.

In conclusion, the CNN, which is designed specifically based on the characters of the brain images, combined with the pre- and post- processing blocks, performs the brain tumor segmentation precisely and efficiently with a very low computation cost.

### III. PERFORMANCE EVALUATION

The proposed system for brain tumor segmentation has been trained and tested with a commonly used dataset, namely BRATS2018, for its performance evaluation. The details of the training and testing processes are presented in the following subsections.

#### A. Dataset and Training Process

##### 1) Dataset

The dataset BRATS2018 includes all of the samples from BRATS2017 dataset and part of the samples from BRATS2015. The number of patient cases and the partition of training/test

sets are shown in Table II.

TABLE II  
PARTITION OF THE SAMPLES FROM DATASET BRATS2018

Dataset	Number of patient cases for training		Number of patient cases for testing
	HGG	LGG	
BRATS2018	210	75	66

As the number of patient cases from the dataset is very limited, data augmentation has been performed to have a decent training process. It was done by up-down and left-right flipping each slice in all the 3D brain images in the training set. Moreover, in order to include slices of different texture pattern in each batch, the slices in the training set have been sorted by shuffling them randomly.

##### 2) Training Details

In the proposed CNN, there are 11716 parameters to be determined by means of training process. A number of elements are critical for the quality of the training:

1. Batch size and the number of training epochs. The batch size is chosen to be 100, and the training process is completed after 50 epochs.
2. Learning rate. Cosine Decay [21] is chosen to make the learning rate variable from 0.01 to  $1 \times 10^{-6}$ . In this way, the system loss is reduced coarsely and quickly during the first epochs and is then adjusted finely in the last epochs.
3. Loss function. The loss function is chosen to be Cross Entropy [22].
4. Optimizer. The optimizer is chosen to be Adaptive Moment Estimation (Adam) [23].
5. Initialization. The initial weights are chosen to be truncated normal distribution with 0.1 standard deviation, and the initial biases are chosen to be 0.1.

The loss curve of training process of the proposed system is

shown in Fig. 9. It has been confirmed that the loss is reduced quickly during the first 10 epochs, and only 50 epochs are needed to complete the training process.

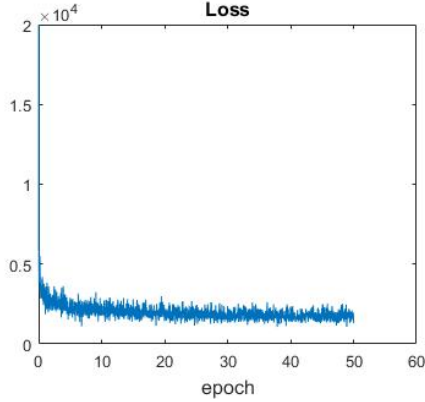


Fig. 9. Loss curve in the training process of the proposed system.

## B. Testing and Performance Evaluation

After determining the values of the trainable parameters in the CNN by the training process, the proposed system has been tested by using BRATS2018 test (validation) set. To have the results of evaluation formally recognized, the output data of the proposed system have been examined by CBICA Image Processing Portal [24], an online evaluation platform, where the assessment is a standard process with data from the Cancer Imaging Archive [25][26].

### 1) Performance Metrics

There are four commonly used metrics to evaluate the segmentation quality, namely Dice score (*Dice*), Sensitivity (*Sens*), Specificity (*Spec*) and Hausdorff95 distance (*Haus*) [1]. The first three metrics are defined as follows.

$$Dice(P_1, T_1) = \frac{|P_1 \wedge T_1|}{(|P_1| + |T_1|)/2} \quad (1)$$

$$Sens(P_1, T_1) = \frac{|P_1 \wedge T_1|}{|T_1|} \quad (2)$$

$$Spec(P_0, T_0) = \frac{|P_0 \wedge T_0|}{|T_0|} \quad (3)$$

where  $P_0$  and  $P_1$  are the predicted results, indicating the number of voxels in the tumor-free regions and that in the tumor regions, respectively, as shown in Fig. 10, whereas  $T_0$  and  $T_1$  are those in the ground truth. In addition, *Haus* is used to indicate the distance between the predicted tumor boundaries and those of the ground truth [1].

As the tumor voxels take a very small portion of space in a 3D brain image, we have

$$P_1 \ll P_0, \quad T_1 \ll T_0, \quad P_0 \approx T_0 \approx |P_0 \wedge T_0|, \\ Spec(P_0, T_0) \approx 1$$

As  $Spec(P_0, T_0)$  is almost equal to unit in most of brain tumor segmentation cases, it does not indicate sensitively a difference in identification of true/false negative voxels.

To better evaluate the quality of the segmentation in different aspects, the metrics of False Discovery Rate (*FDR*) [27] and False Negative Rate (*FNR*, or miss rate) [28] of the proposed system have also been measured. False Discovery Rate (*FDR*) is the ratio of the number of false positive voxels to the total number of predicted positive voxels, indicating how many

voxels are falsely predicted to be positive, whereas *FNR*, or miss rate, is the ratio of the number of false negative voxels to the total number of positive voxels in the ground truth. They are expressed as follows.

$$FDR(P_1, T_1) = \frac{P_1 - |P_1 \wedge T_1|}{P_1} \\ = 1 - \frac{1}{2/Dice(P_1, T_1) - 1/Sens(P_1, T_1)} \quad (4)$$

$$FNR(P_1, T_1) = \frac{T_1 - |P_1 \wedge T_1|}{T_1} \\ = 1 - Sens(P_1, T_1) \quad (5)$$

The performance metrics of a CNN system also include measures of the computation volume required to achieve the processing quality, as it is related to the computation efficiency, the feasibility of system implementations, and the range of applications. The number of parameters in the CNN is an important indicator of the computation volume in both training and testing process. The number of floating-point operations (FLOPs) required to complete a test for one patient case is related to the applications of the system, as it determines where the system can be installed and how fast the process will be.

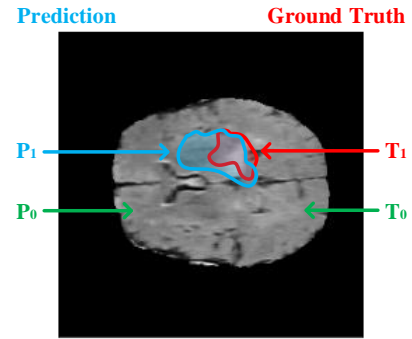


Fig. 10. Slice of segmented brain image to indicate the lesion.  $T_1$  is the number of pixels in the true lesion region, which is located in the red-contoured area.  $P_1$  is the number of pixels in predicted lesion region, which is located in the blue-contoured area.  $T_0$  and  $P_0$  are the number of pixels in normal regions in the ground truth and the predicted maps, respectively.

### 2) Results

As mentioned previously, the performance assessment of the proposed system has been done with the dataset BRATS2018, and all the results have been generated by CBICA Image Processing Portal. Ten experiments have been conducted. Each experiment has been done by (i) training the system from the initial state and (ii) testing all the 66 test cases in the testing pool and generating 66 results.

If the system is functional, it should deliver the results of high processing quality in a consistent manner. The degree of the consistency reflects the degree of the reliability and confidence of the results. Therefore, the assessment of the consistency in system performance should be part of the validation of the results.

To assess the consistency, the 10 sets of 66-results have been examined in the aspects of the statistical feature data, and the results of individual patient cases obtained in the 10 experiments.

Each of the 66 results from every single experiment includes the 3 *Dice* scores for ET, WT and TC. The mean, median and mode values of the scores have been calculated and presented

in Table III. Each column in the table contains 10 statistical feature data of the same kind, e.g., mean values of ET *Dice* scores, generated in the 10 experiments, and their values are very close to each other. These data demonstrate that the functionality of the system is statistically consistent after any of the 10 training processes.

As the system is functioning in a consistent manner, the *Dice* scores presented in Table III are reliable for the 66 patient cases. The data illustrate that the proposed system is able to deliver high-quality segmentation results. For enhancing tumors, the median *Dice* score is 0.85, and the value of the mode is 0.9. The mean values of all the 3 *Dice* scores are, consistently in all the 10 experiments, lower than the median values. In fact, in all the 10 experiments, only approximately 22% of the 66 patient cases, which is less than the first quantile, have got ET (or WT) *Dice* scores lower than the mean value, and in case of TC *Dice* scores, it has been around 32%. Thus, the mean scores represent more a small minority, than the large majority, of the cases.

The consistency of the performance is also related to the reproducibility of the system in processing individual patient cases. For a given patient case, a functional system should be able to reproduce similar results, if not the same, each time after the system is re-trained from the initial state. The results of 2 cases are presented in Table IV.

TABLE III  
STATISTICAL DATA OF THE TEN EXPERIMENTS

Exp.	<i>Dice</i> - Mean			<i>Dice</i> - Median			<i>Dice</i> - Mode		
	ET	WT	TC	ET	WT	TC	ET	WT	TC
No. 1	0.757	0.887	0.761	0.852	0.918	0.856	0.91	0.93	0.93
No. 2	0.742	0.886	0.766	0.852	0.916	0.862	0.91	0.93	0.93
No. 3	0.752	0.885	0.741	0.850	0.915	0.861	0.89	0.93	0.93
No. 4	0.739	0.884	0.762	0.853	0.916	0.858	0.87	0.93	0.93
No. 5	0.749	0.889	0.761	0.847	0.914	0.856	0.89	0.91	0.95
No. 6	0.746	0.886	0.763	0.853	0.913	0.862	0.91	0.93	0.93
No. 7	0.765	0.884	0.760	0.856	0.915	0.866	0.89	0.91	0.93
No. 8	0.722	0.881	0.754	0.852	0.919	0.859	0.91	0.93	0.93
No. 9	0.748	0.890	0.762	0.852	0.912	0.868	0.89	0.93	0.93
No. 10	0.766	0.877	0.755	0.859	0.917	0.861	0.89	0.93	0.91
Average	0.749	0.885	0.758	0.853	0.916	0.861	0.90	0.93	0.93
STDEV	0.013	0.004	0.007	0.003	0.002	0.004	0.013	0.008	0.009

TABLE IV  
DICE SCORES OF 2 PATIENT CASES

Exp.	<i>Dice</i> - Case 1 *			<i>Dice</i> - Case 2 **		
	ET	WT	TC	ET	WT	TC
No. 1	0.882	0.930	0.923	0.727	0.902	0.829
No. 2	0.885	0.929	0.925	0.736	0.883	0.853
No. 3	0.886	0.929	0.929	0.775	0.882	0.867
No. 4	0.886	0.934	0.883	0.747	0.892	0.863
No. 5	0.892	0.930	0.944	0.756	0.888	0.879
No. 6	0.890	0.932	0.873	0.731	0.884	0.857
No. 7	0.890	0.929	0.904	0.759	0.879	0.855
No. 8	0.881	0.931	0.908	0.753	0.903	0.870
No. 9	0.893	0.929	0.882	0.764	0.898	0.859
No. 10	0.887	0.930	0.913	0.722	0.886	0.858
Average	0.887	0.930	0.908	0.747	0.890	0.859
STDEV	0.004	0.002	0.023	0.017	0.009	0.013

\*: Case 1: Brats18\_MDA\_922\_1.

\*\* Case 2: Brats18\_MDA\_907\_1.

The *Dice* scores of Case 1 in Table IV are excellent. It should, however, be noted that such scores are the most frequently appearing in testing the 66 cases, as indicated by the values of *Dice* - mode, shown in Table III. For this patient case, the ten experiments have generated almost the same scores, with standard deviations of 0.004, 0.002 and 0.023 for *Dice* scores of ET, WT and TC, respectively. Case 2 is among the minority of the 66 cases that got low *Dice* scores, and its scores obtained in the 10 experiments are also quite consistent. A similar level of consistency has also been observed in the test results of the other individual cases, regardless the levels of their *Dice* scores. One can conclude that the proposed CNN system has a very good reproducibility of the results to the same inputs.

The assessment results of the proposed system are compared with those produced by seven other CNN systems having moderate complexity and reported in recent years. The mean scores of *Dice*, *Sensitivity*, *Specificity* and *Hausdorff95* of the proposed system, together with those of the seven systems, are presented in Table V. The results of False Discovery Rate (*FDR*), False Negative Rate (*FNR*), and the measures of computation complexity are found in Table VI. As training/testing samples play very important role in the performance evaluation, for each of the systems listed for comparison, the information about which datasets were used and whether the results were generated by CBICA Image Processing Portal is also found in the two tables.

It should be underlined that, the CNN block in the proposed system requires only 11.716K parameters for its 7 convolution layers, as shown in Table VI. Its computation cost is significantly lower than those reported so far, and the system yields, nevertheless, a high processing quality. One can easily see that, compared with other brain tumor segmentation systems of modest computation, the proposed system has:

1. Very good *Dice* scores,
2. the lowest False Discovery Rates (*FDR*) in the detection of ET, WT and TC,
3. False Negative Rates (*FNR*) or miss rates are comparable to others, and
4. the best results in the detection of ET voxels in the aspects of *Dice* and *FDR*. In particular, the *FDR* of ET is 10% lower than the second best found in the list.

The excellent processing quality is mainly owing to the specifically designed CNN for brain tumor segmentation. Though it has only 7 convolution layers, the operations in each layer is made to extract critical feature information, first for the localization of the tumor areas and then for the precise classification. Furthermore, the refinement block provides another improvement, after the CNN, in the ET detection: The average of *Dice* scores is increased from 72.2% to 74.9%, that of *FDR* reduced from 32.4% to 28.0% and *Hausdorff95* reduced from 7.3 to 5.0.



TABLE V  
COMPARISON OF THE RESULTS – DICE, SENSITIVITY, SPECIFICITY AND HAUSDORFF95

Systems	Dataset (BRATS)	Assessed by CBICA	Dice			Sensitivity			Specificity			Hausdorff95		
			ET	WT	TC	ET	WT	TC	ET	WT	TC	ET	WT	TC
Ding et al. [9]	2015	No	0.592	0.831	0.671	N.A.	N.A.	N.A.	N.A.	N.A.	N.A.	N.A.	N.A.	N.A.
Ding et al. [12]	2015	No	0.63	0.86	0.71	N.A.	N.A.	N.A.	N.A.	N.A.	N.A.	N.A.	N.A.	N.A.
Li et al. [8]	2017	No	0.642	0.876	0.763	N.A.	N.A.	N.A.	N.A.	N.A.	N.A.	N.A.	N.A.	N.A.
Pereira et al. [11]	2017	Yes	0.733	0.895	0.798	N.A.	N.A.	N.A.	N.A.	N.A.	N.A.	5.074	5.920	8.947
Chen et al. [15]	2017	Yes	0.7346	0.8930	0.7388	N.A.	N.A.	N.A.	N.A.	N.A.	N.A.	N.A.	N.A.	N.A.
Chen et al. [10]	2017	No	0.6498	0.8347	0.7321	0.8035	0.8453	0.7493	0.9994	0.9986	0.9992	30.3100	36.4000	25.5900
Hu et al. [13]	2018	Yes	0.7178	0.8824	0.7481	0.8684	0.9074	0.7621	0.9947	0.9918	0.9969	5.6864	12.6069	9.6223
<b>Proposed</b>	<b>2018</b>	<b>Yes</b>	<b>0.7486</b>	<b>0.8849</b>	<b>0.7583</b>	<b>0.7797</b>	<b>0.8757</b>	<b>0.7580</b>	<b>0.9978</b>	<b>0.9949</b>	<b>0.9968</b>	<b>5.0232</b>	<b>6.4887</b>	<b>10.7027</b>

TABLE VI  
COMPARISON OF THE RESULTS – FDR, FNR, COMPUTATION COMPLEXITY/VOLUME

System	Dataset (BRATS)	False Discovery Rate			False Negative Rate			Max number of filters in a layer	Number of layers	Number of Parameters	Number of FLOPs per patient case
		ET	WT	TC	ET	WT	TC				
Ding et al. [9]	2015	N.A.	N.A.	N.A.	N.A.	N.A.	N.A.	256	approx. 29	6.66M	N.A.
Ding et al. [12]	2015	N.A.	N.A.	N.A.	N.A.	N.A.	N.A.	512	approx. 25	N.A.	N.A.
Li et al. [8]	2017	N.A.	N.A.	N.A.	N.A.	N.A.	N.A.	N.A.	approx. 17	N.A.	N.A.
Pereira et al. [11]	2017	N.A.	N.A.	N.A.	N.A.	N.A.	N.A.	160	approx. 24	N.A.	N.A.
Chen et al. [15]	2017	N.A.	N.A.	N.A.	N.A.	N.A.	N.A.	164	11	100K	N.A.
Chen et al. [10]	2017	0.4545	0.1756	0.2843	0.1965	0.1547	0.2507	N.A.	N.A.	10.03M	N.A.
Hu et al. [13]	2018	0.3883	0.1413	0.2654	0.1316	0.0926	0.2379	160	approx. 39	N.A.	N.A.
<b>Proposed</b>	<b>2018</b>	<b>0.2801</b>	<b>0.1057</b>	<b>0.2414</b>	<b>0.2203</b>	<b>0.1243</b>	<b>0.2420</b>	<b>16</b>	<b>7</b>	<b>11.716K</b>	<b>21.14G</b>

Another important item in the performance metrics is the number of floating-point operations (FLOPs) required to complete the segmentation of each patient case. With a large amount of input data, i.e., 35.712M ( $240 \times 240 \times 155 \times 4$ ) voxels in 3D brain MRI images in each patient case, the proposed CNN requires only 21.14G FLOPs to complete the task. This extremely small number of FLOPs results mainly from the simplicity of the proposed CNN with 11.716K parameters. Also, the pre-processing block helps to reduce more than 50% of the input data volume applied to the CNN.

The testing results confirm that, though the proposed system is very simple in structure and has very low computation complexity, its processing quality is very high, which, in fact, thanks to the efficient filtering operations in its specifically designed convolution layers. The results also confirm that the pre- and post-processing blocks efficiently contribute to the high performance. The most important of all is, nevertheless, that the proposed system is able to operate with a high degree of consistency and to reproduce its results in a reliable manner.

#### IV. CONCLUSION

In this paper, a computation-efficient CNN system has been proposed for brain tumor segmentation. The system is very simple and custom-designed to operate with 3D brain images to achieve high processing quality at the lowest computation cost. It is composed of three parts, a pre-processing block to reduce the data volume, a very simple CNN to segment tumor areas precisely, and a refinement block to detect false positive pixels. The CNN has 7 convolution layers and 16 output channels per

layer, except the last one, requiring only 11716 parameters in total. The convolutions combined with max pooling in the first half of the CNN are to localize brain tumor areas. Two convolution modes, namely depthwise convolution and standard convolution, are performed in parallel in the first 2 layers to extract elementary features efficiently. In the second half of the CNN, the convolutions combined with upsampling are to segmentation tumor areas in pixel-wise precision. For a fine classification, the feature maps are modulated by adding the local feature maps generated in the first half of the CNN.

The performance of the proposed system has been tested with BRATS2018 dataset. Multiple experiments have been done to assess not only the processing quality, but also the consistency in performance. The test results have been generated by CBICA Image Processing Portal. It has been demonstrated that the system reproduces almost the same results to a given patient case every time after it is re-trained. The test results have been compared with those of the CNNs of moderate complexity reported in recent years. The overall processing quality of the propose system is comparable to the best ones so far reported. In particular, in the aspect of detecting enhancing tumor, it gives the best Dice score and the lowest False Discovery Rate. Requiring only 11716 parameters, the proposed system can be very easily trained and implemented in computation-restricted environments. Hence, a wide range of applications can be expected.

It should be mentioned that the proposed system is not for general purpose. It has been designed to meet the specific needs to segment brain tumors or other kinds of tumors in medical images. In this way, the redundancy in computation can be

minimized, the information density in data flow increased, and the computation efficiency/quality improved. This design demonstrates that a CNN system can be made to perform a high-quality processing, at a very low computation cost, for a specific application. Hence, application-specific CNN (ASCNN) is an effective approach to lowering the barrier of computation resource requirement of CNN systems to make them more implementable and applicable for general public.

## REFERENCES

- [1] B. H. Menze et al., "The Multimodal Brain Tumor Image Segmentation Benchmark (BRATS)," *IEEE Trans. Med. Imag.*, vol. 34, no. 10, pp. 1993-2024, Oct. 2015.
- [2] P. Gibbs, D. L. Buckley, S. J. Blackband, and A. Horsman, "Tumour volume determination from MR images by morphological segmentation," *Phys. Med. Biol.*, vol. 41, no. 11, pp. 2437-2446, 1996.
- [3] T. Imtiaz, S. Rifat, S. A. Fattah and K. A. Wahid, "Automated Brain Tumor Segmentation Based on Multi-Planar Superpixel Level Features Extracted From 3D MR Images," *IEEE Access*, vol. 8, pp. 25335-25349, 2020.
- [4] N. Geschwind and W. Levitsky, "Human Brain: Left-right asymmetry in temporal speech region," *Science*, vol. 161, pp. 186-187, 1968.
- [5] A. Kermi, K. Andjouh and F. Zidane, "Fully automated brain tumour segmentation system in 3D-MRI using symmetry analysis of brain and level sets," *IET Image Processing*, vol. 12, no. 11, pp. 1964-1971, 11 2018.
- [6] J. Long, E. Shelhamer and T. Darrell, "Fully convolutional networks for semantic segmentation," *2015 IEEE Conference on Computer Vision and Pattern Recognition (CVPR)*, Boston, MA, 2015, pp. 3431-3440.
- [7] O. Ronneberger, P. Fischer, and T. Brox, "U-net: Convolutional networks for biomedical image segmentation," *Proc. MICCAI*, Nov. 2015, pp. 234-241.
- [8] Haichun Li, Ao Li and Minghui Wang, "A novel end-to-end brain tumor segmentation method using improved fully convolutional networks," *Computers in Biology and Medicine*, vol. 108, p. 150-160, May 2019.
- [9] Y. Ding, F. Chen, Y. Zhao, Z. Wu, C. Zhang and D. Wu, "A Stacked Multi-Connection Simple Reducing Net for Brain Tumor Segmentation," *IEEE Access*, vol. 7, pp. 104011-104024, 2019.
- [10] L. Chen, P. Bentley, K. Mori, K. Misawa, M. Fujiwara and D. Rueckert, "DRINet for Medical Image Segmentation," *IEEE Trans. Med. Imag.*, vol. 37, no. 11, pp. 2453-2462, Nov. 2018.
- [11] S. Pereira, A. Pinto, J. Amorim, A. Ribeiro, V. Alves and C. A. Silva, "Adaptive feature recombination and recalibration for semantic segmentation with Fully Convolutional Networks," *IEEE Trans. Med. Imag.*, May 2019.
- [12] Y. Ding, C. Li, Q. Yang, Z. Qin and Z. Qin, "How to Improve the Deep Residual Network to Segment Multi-Modal Brain Tumor Images," *IEEE Access*, vol. 7, pp. 152821-152831, 2019.
- [13] K. Hu et al., "Brain Tumor Segmentation Using Multi-Cascaded Convolutional Neural Networks and Conditional Random Field," *IEEE Access*, vol. 7, pp. 92615-92629, Jul. 2019.
- [14] K. Kamnitsas, C. Ledig, V.F. Newcombe, J.P. Simpson, A.D. Kane, D.K. Menon, D. Rueckert, B. Glocker, "Efficient multi-scale 3D CNN with fully connected CRF for accurate brain lesion segmentation," *Med. Image Anal.*, vol. 36, pp. 61-78, 2017.
- [15] Chen, Shengcong, Ding, Changxing and Liu, Minfeng, "Dual-force convolutional neural networks for accurate brain tumor segmentation," *Pattern Recognition*, vol. 88, pp. 90-100, Apr. 2019.
- [16] Tuzikov, A., Colliot, O., Bloch, I. "Evaluation of the symmetry plane in 3D MR brain images," *Pattern Recognit Lett.*, 2003, 24, pp. 2219-2233.
- [17] S. Prima, S. Ourselin and N. Ayache, "Computation of the mid-sagittal plane in 3-D brain images," *IEEE Trans. Med. Imag.*, vol. 21, no. 2, pp. 122-138, Feb. 2002.
- [18] Zhou Wang, A. C. Bovik, H. R. Sheikh and E. P. Simoncelli, "Image quality assessment: from error visibility to structural similarity," *IEEE Trans. Image Process.*, vol. 13, no. 4, pp. 600-612, April 2004.
- [19] L. Nyúl and J. Udupa, "On standardizing the MR image intensity scale," *Magn. Reson. Med.*, vol. 42, no. 6, pp. 1072-1081, 1999.
- [20] L. G. Nyúl, J. K. Udupa, and X. Zhang, "New variants of a method of MRI scale standardization," *IEEE Trans. Med. Imag.*, vol. 19, no. 2, pp. 143-150, Feb. 2000.
- [21] I. Loshchilov and F. Hutter, "Sgdr: stochastic gradient descent with restarts," *International Conference on Learning Representations 2016*, 2016.
- [22] Y. LeCun, Y. Bengio, and G. Hinton, "Deep learning," *Nature*, vol. 521, no. 7553, p. 436-444, 2015.
- [23] Diederik P. Kingma, Jimmy Ba, "Adam: A method for stochastic optimization", *arXiv:1412.6980*, 2014.
- [24] <https://www.med.upenn.edu/sbia/brats2018/data.html>
- [25] S. Bakas et al., "Advancing The Cancer Genome Atlas glioma MRI collections with expert segmentation labels and radiomic features", *Nature Scientific Data*, 4:170117 (2017) DOI: 10.1038/sdata.2017.117.
- [26] S. Bakas et al., "Identifying the Best Machine Learning Algorithms for Brain Tumor Segmentation, Progression Assessment, and Overall Survival Prediction in the BRATS Challenge", *arXiv preprint arXiv:1811.02629* (2018).
- [27] Yoav Benjamini and Yosef Hochberg. "Controlling the False Discovery Rate: A Practical and Powerful Approach to Multiple Testing," *Journal of the Royal Statistical Society. Series B (Methodological)*, vol. 57, no. 1, pp. 289-300, 1995.
- [28] Ralph M. Richart M. D. "Evaluation of the true false negative rate in cytology," *American Journal of Obstetrics and Gynecology*, vol. 89, no. 6, pp. 723-726, July 1964.